Nuclear Inst. and Methods in Physics Research, A 935 (2019) 173–177

Contents lists available at ScienceDirect

Nuclear Inst. and Methods in Physics Research, A

journal homepage: www.elsevier.com/locate/nima

From optical to X-ray ghost imaging

Thomas A. Smith [a,*], Yanhua Shih [a], Zhehui Wang [b], Xuan Li [b], Bernhard Adams [c], Marcel Demarteau [d], Robert Wagner [d], Junqi Xie [d], Lei Xia [d], Ren-Yuan Zhu [e], Liyuan Zhang [e], Chen Hu [e]

[a] Department of Physics, University of Maryland, Baltimore County, Baltimore, MD 21250, USA
[b] Los Alamos National Laboratory, Los Alamos, NM 87545, USA
[c] Incom, Inc., Charlton, MA 01507, USA
[d] Argonne National Laboratory, Lemont, IL 60439, USA
[e] 256-48, HEP, California Institute of Technology, Pasadena, CA 91125, USA

ARTICLE INFO

Keywords:
Optics
Imaging
Quantum optics
Ghost imaging
X-rays
Synchrotron

ABSTRACT

Recent advances in ghost imaging techniques and X-ray sources such as synchrotrons and, more recently, X-ray free-electron lasers (XFEL) have made X-ray ghost imaging a growing topic of interest. One specific type of ghost imaging utilizes thermal radiation and the measurement of intensity fluctuation correlation to form a true image without the need of a lens. This technique allows for much higher resolution than traditional X-ray imaging for a mesoscopic or even a microscopic object. In addition to this benefit of not requiring a lens, a surprising experiment has shown that, when set up correctly, this type of ghost imaging can provide clear images through the measurement of intensity fluctuation correlation when traditional images through measurements of intensity are blurred due to optical turbulence and vibrations. This turbulence-free technique will help maintain the high resolution of X-ray ghost imaging. How is an image formed from fluctuations in light? And what makes it turbulence-free? Using the concept of two-photon interference, this article provides an introduction to these fundamentally interesting concepts and X-ray ghost imaging.

Contents

1. Introduction

The first demonstration of ghost imaging was accomplished by Pittman et al. with the measurement of coincidence counts of entangled photon pairs incident on two separate detectors [1]. Shortly following, efforts were made to develop ghost imaging with thermal light [2]. Due to how common thermal light is (generated by the sun, light bulbs, and many other sources), ghost imaging with thermal light is more accessible than ghost imaging with entangled light. Valencia et al. were able to achieve ghost imaging with thermal light through the measurement of intensity fluctuation correlation. Unlike mean intensity measurements, which is a result of single-photon interference, intensity fluctuation correlation is a measurement of two-photon interference, or a pair of photons interfering with the pair itself [3]. This type of ghost imaging also does not require the use of a lens, as the image is formed directly from the correlation. Taking advantage of this feature, we can extend ghost imaging to X-ray regime which have much higher penetrating power than optical photons and are unaffected by traditional lenses. Applying X rays will allow for higher resolution images, with the potential for angstrom-level resolution.

To model ghost imaging and two-photon interference, we will utilize Einstein's theory of light. Einstein introduced granularity to light by theorizing that, instead of long, continuous electromagnetic waves, it consisted of many individual subfields (now known as photons) emitted

* Corresponding author.
E-mail address: tsmith25@umbc.edu (T.A. Smith).

https://doi.org/10.1016/j.nima.2019.05.027
Received 8 December 2018; Received in revised form 24 April 2019; Accepted 8 May 2019
Available online 11 May 2019
0168-9002/

by many subsources (now known as atomic transitions) [4]. For thermal light (which is used throughout this paper), these subfields are emitted randomly with a random phase. While the quantum picture would adequately explain these phenomena, it has been shown that the effective wave function of a photon in the thermal state is mathematically the same function as Einstein's subfield model, so we will focus on the latter [5–8]. When many subfields, represented by E_m, are present at one location, the total electric field is the superposition of each subfield,

$$E(\mathbf{r},t) = \sum_m E_m(\mathbf{r},t) = \sum_m \int d\omega E_m(\omega) g_m(\omega;\mathbf{r},t), \tag{1}$$

for which

$$E_m(\omega) = a_m(\omega) e^{i\phi_m(\omega)}, \tag{2}$$

where $a_m(\omega)$ is the amplitude and $\phi_m(\omega)$ is the random initial phase of the subfield. The Green's function, $g_m(\omega;\mathbf{r},t)$, is used as a "propagator" which represents propagations from the mth subsource located at $(\mathbf{r}_m, t_m)$ to a separate point in spacetime at $(\mathbf{r},t)$. The Green's function varies depending on the path of propagation. Here we will approximate ghost imaging as a near field measurement and also only focus on the spatial portion of the Green's function. Written in terms of the transverse coordinate $\boldsymbol{\rho}$, the near-field spatial Green's function is

$$g_m(\omega;\boldsymbol{\rho},z) = \frac{-i\omega}{2\pi c}\frac{e^{i\frac{\omega}{c}z}}{z} e^{i\frac{\omega}{2cz}|\boldsymbol{\rho}-\boldsymbol{\rho}_m|^2}. \tag{3}$$

The measurement of intensity at a single detector located at $(\mathbf{r},t)$, is represented by the expectation value or ensemble average of intensity, $\langle I(\mathbf{r},t)\rangle$. Intensity is an amplitude–amplitude correlation which, using Glauber's formalism, is also known as first order correlation, $\Gamma^{(1)}(\mathbf{r},t)$. This measurement is the total electric field correlated with itself, thus correlating all of the subfields with themselves ($m = n$) *and* all others ($m \neq n$). It is convenient to split our intensity term into these two separate cases,

$$\begin{aligned}\Gamma^{(1)}(\mathbf{r},t) &= \langle I(\mathbf{r},t)\rangle = \left\langle E^*(\mathbf{r},t)E(\mathbf{r},t)\right\rangle \\ &= \Big\langle \sum_m E_m^*(\mathbf{r},t) \sum_n E_n(\mathbf{r},t)\Big\rangle \\ &= \Big\langle \sum_m \left|E_m(\mathbf{r},t)\right|^2\Big\rangle + \Big\langle \sum_{m\neq n} E_m^*(\mathbf{r},t)E_n(\mathbf{r},t)\Big\rangle \\ &= \sum_m \left|E_m(\mathbf{r},t)\right|^2 + 0.\end{aligned} \tag{4}$$

When the intensity of thermal light is large enough (or the time window long enough) all random phases may be present in the measurement causing the $m \neq n$ terms to sum to zero, leaving just the $m = n$ terms (for which the initial phase information cancels before the summation). Even when present, the $m \neq n$ terms are simply considered as noise, or fluctuations about the mean intensity,

$$\langle I(\mathbf{r},t)\rangle = \bar{I}(\mathbf{r},t) + \Delta I(\mathbf{r},t). \tag{5}$$

Traditional imaging processes and interferometers are a result of the mean intensity term, or subfields correlated with themselves. This coincides with Dirac's observation that a photon only interferes with itself [9].

2. Two-photon interference

By introducing a second detector, intensity correlation measurements can be made such as those demonstrated by Hanbury Brown and Twiss in their stellar interferometer [10,11]. Using Glauber's formalism, this is known as second order correlation, $\Gamma^{(2)}(\mathbf{r}_1,t_1;\mathbf{r}_2,t_2)$. Like with intensity, the cancellation of the initial phase terms is required to survive the ensemble average. In this case there are two sets of terms that survive: (1) when $m = n$ and $p = q$, and (2) when $m = q$ and $n = p$.

$$\begin{aligned}\Gamma^{(2)}(\mathbf{r}_1,t_1;\mathbf{r}_2,t_2) &= \langle I(\mathbf{r}_1,t_1)I(\mathbf{r}_2,t_2)\rangle \\ &= \left\langle E^*(\mathbf{r}_1,t_1)E(\mathbf{r}_1,t_1)E^*(\mathbf{r}_2,t_2)E(\mathbf{r}_2,t_2)\right\rangle \\ &= \Big\langle \sum_m E_m^*(\mathbf{r}_1,t_1)\sum_n E_n(\mathbf{r}_1,t_1)\sum_p E_p^*(\mathbf{r}_2,t_2)\sum_q E_q(\mathbf{r}_2,t_2)\Big\rangle \\ &= \sum_m \left|E_m(\mathbf{r}_1,t_1)\right|^2 \sum_n \left|E_n(\mathbf{r}_2,t_2)\right|^2 \\ &\quad + \sum_{m\neq n} E_m^*(\mathbf{r}_1,t_1)E_n(\mathbf{r}_1,t_1)E_n^*(\mathbf{r}_2,t_2)E_m(\mathbf{r}_2,t_2) \\ &= \bar{I}(\mathbf{r}_1,t_1)\bar{I}(\mathbf{r}_2,t_2) + \langle \Delta I(\mathbf{r}_1,t_1)\Delta I(\mathbf{r}_2,t_2)\rangle.\end{aligned} \tag{6}$$

It is evident that the $m = n$ and $p = q$ terms correspond to the mean intensities measured at each respective detector, D_1 and D_2. The remaining $m = q$ and $n = p$ terms are simply the correlation of the intensity fluctuation term for D_1 and the intensity fluctuation term for D_2,

$$\langle \Delta I(\mathbf{r}_1,t_1)\Delta I(\mathbf{r}_2,t_2)\rangle = \sum_{m\neq n} E_m^*(\mathbf{r}_1,t_1)E_n(\mathbf{r}_1,t_1)E_n^*(\mathbf{r}_2,t_2)E_m(\mathbf{r}_2,t_2). \tag{7}$$

Earlier we stated that the fluctuation term either averages to zero or contributes unwanted noise to the measurement of intensity; however, here we see that this is not the case for intensity fluctuation correlation. The phase information cancels in this measurement, allowing it to survive the ensemble average. Experimentally this can be obtained by measuring the intensity in a series of short time windows at two separate detectors. After obtaining the mean intensity, the fluctuation at each of the time windows can be determined. Then these individual fluctuation terms are correlated with the corresponding terms of the other detector. Averaging these correlated terms gives the final value.

This measurement can be explained as a result of two-photon interference [3]. Comparable to single-photon interference which is apparent through the measurement of intensity (Eq. (4)), two-photon interference is a result of a pair of photons interfering with the pair itself. To better visualize this, we can rewrite Eq. (6) as the following superposition [3],

$$\begin{aligned}&\langle I(\mathbf{r}_1,t_1)I(\mathbf{r}_2,t_2)\rangle \\ &\quad = \sum_{m\neq n}\frac{1}{2}\left|E_m g_m(\mathbf{r}_1,t_1)E_n g_n(\mathbf{r}_2,t_2) + E_m g_m(\mathbf{r}_2,t_2)E_n g_n(\mathbf{r}_1,t_1)\right|^2\end{aligned}$$

Here we clearly see it describes two probability amplitudes for joint detection: (1) the mth subfield is detected at detector 1 while the nth subfield is detected at detector 2, *or* (2) the nth subfield is detected at detector 1 while the mth subfield is detected at detector 2. The cross terms of this superposition are equivalent to the intensity fluctuation correlation and, in the quantum description, represent the two probability amplitudes interfering with one another.

To better understand the phenomena of two-photon interference, it may be useful to review the turbulence-free two-photon double-slit interferometer that has been recently developed [12]. Although not required, a coherent source like a laser is typically used for a classic double-slit interferometer. It becomes more difficult to produce an interference pattern in the measurement of intensity with thermal light due to the spatial coherence of the source: if the source is too large and the slit separation is greater than the spatial coherence length ($d \gg l_c$), the light will be incoherent and not produce an interference pattern [7,13]. However, two-photon interference through the measurement of intensity fluctuation correlation is able to produce a fully visible interference pattern even with fully incoherent light, $d \gg l_c$.

When using an incoherent, thermal light source, there are multiple two-photon amplitudes contributing to the measurement of intensity fluctuation correlation. Two alternatives that produce an interference pattern are when the mth subfield propagates from slit-A to detector 1 while the nth subfield propagates from slit-B to detector 2, *or* the mth subfield propagates from slit-A to detector 2 while the nth subfield propagates from slit-B to detector 1. These two-photon probability

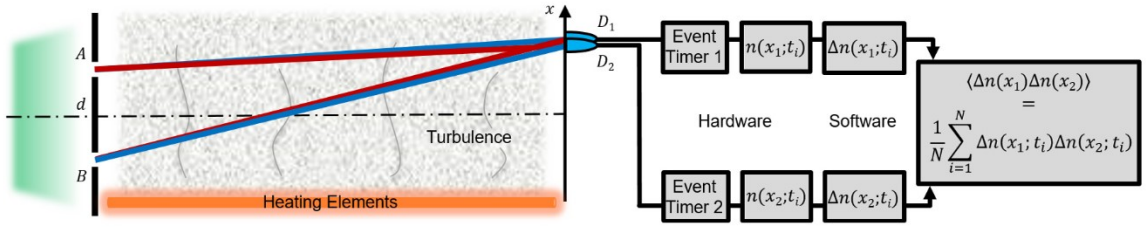

Fig. 1. The observed interference is a two-photon phenomenon: a random pair of photons interfering with the pair itself. In the figure, the superposed two different, yet indistinguishable two-photon amplitudes are indicated by red and blue colors. When the detectors are scanning in the neighborhood of $x_1 \approx x_2$, the red amplitude and the blue amplitude "overlap". This overlap means the pair experience the same phase variations in the red-path and the blue-path. Therefore, the interference will be unaffected by the turbulence. (For interpretation of the references to color in this figure legend, the reader is referred to the web version of this article.)

amplitudes are depicted in Fig. 1 in blue and red, respectively. This superposition results in,

$$\langle \Delta I_{AB}(x_1)\Delta I_{AB}(x_2)\rangle = \sum_{m\neq n} |E_m|^2|E_n|^2 g^*_{mA}(x_1)g_{nB}(x_1)g_{mA}(x_2)g^*_{nB}(x_2) \propto \cos\frac{2\pi d}{\lambda z}(x_1 - x_2). \quad (8)$$

In addition to the above alternatives for the mth and the nth subfields to produce a joint photodetection event of D_1 and D_2, the mth and the nth subfields can also produce a joint photodetection even when both pass through slit-A or both pass through slit-B. These two alternatives contribute constants to $\langle \Delta I(x_1)\Delta I(x_2)\rangle$. Adding the contributions from all alternatives, we have an observable

$$\langle \Delta I(x_1)\Delta I(x_2)\rangle \propto \left[1 + \cos\frac{2\pi d}{\lambda z}(x_1 - x_2)\right]. \quad (9)$$

In general, this measurement may be sensitive to turbulence because the random phase shifts present due to random fluctuations in index of refraction may be different for each path. Mathematically we can represent the turbulence as a random phase shift dependent on the path traveled by the subfield. Introducing this to Eq. (8) we get,

$$\langle \Delta I_{AB}(x_1)\Delta I_{AB}(x_2)\rangle = \sum_{m\neq n} |E_m|^2|E_n|^2 g^*_{mA}(x_1)e^{i\delta\phi_A(x_1)}g_{nB}(x_1)e^{-i\delta\phi_B(x_1)} \times g_{mA}(x_2)e^{-i\delta\phi_A(x_2)}g^*_{nB}(x_2)e^{i\delta\phi_B(x_2)} \quad (10)$$

However, a closer look reveals that there is the possibility for cancellation. By scanning D_1 in approximately the same location as D_2 ($x_1 \approx x_2$), it is clear that the pair of two-photon amplitudes, red and blue, overlap (Fig. 1) [12]. Even though each path involves turbulence, the pair of potential paths for the two-photon experience it by the same magnitude. The resulting interference pattern is unaffected and maintains full visibility.

3. Thermal light ghost imaging

Thermal light ghost imaging, shown in Fig. 2, also utilizes a pair of detectors and the measurement of intensity fluctuation correlation [2]. Here a beam splitter splits light from a thermal source into two paths. One path contains the object of interest (in this case an arbitrary aperture) followed by a bucket detector which ideally collects all of the light from the object. There is no "resolution" needed for this detector so this measurement can be done with a lens focusing all of the light into a single detector or an array of detectors (such as a CCD or CMOS array) for which the measurement from each location is later summed to a single value. The other path from the beam splitter *does* require spatial information, so a full detector array is used. We will define the array of detectors as D_1 and the bucket detector as D_2. For the image to be in focus, the detector array is placed the same distance from the source (or beam splitter) as the object, $z_1 = z_2 \equiv d$. Applying this constraint, the intensity fluctuation correlation produces a sombrero function [7],

$$\langle \Delta I(\rho_1)\Delta I(\rho_2)\rangle \propto \int d\rho_o \left|A(\rho_o)\right|^2 \mathrm{somb}^2\left[\frac{R_s}{d}\frac{\omega}{c}\left|\rho_1 - \rho_o\right|\right], \quad (11)$$

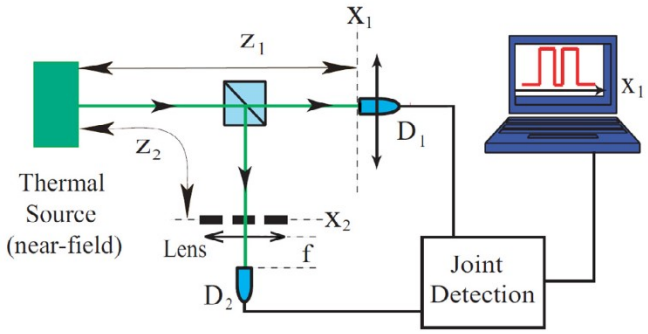

Fig. 2. The setup for thermal light ghost imaging consists of a thermal source of radiation, a beam splitter, a scanning point-like detector or detector array, and a bucket detector (shown here as a lens collecting the light to a single detector). The bucket detector collects all of the light from the object as a single measurement while the detector array does not have a view of object at all.

where R_s is the radius of the source and the sombrero (somb) function is defined as $somb(x) = 2J_1(x)/x$ where $J_1(x)$ is the first-order Bessel function. The somb function is the image forming function, transferring a single point on the object to a "spot" on the image plane. For a source with a large angular diameter, $\Delta\theta_s = R_s/d$, the point-to-spot somb function can be approximated as a point-to-point delta function,

$$\langle \Delta I(\rho_1)\Delta I(\rho_2)\rangle \propto \int d\rho_o \left|A(\rho_o)\right|^2 \delta(\rho_1 - \rho_o) = \left|A(\rho_1)\right|^2. \quad (12)$$

Similar to the turbulence-free double-slit interference pattern, if D_1 and D_2 are arranged in such away to achieve path overlap, the measurement of ghost imaging with thermal light will be insensitive to turbulence. This turbulence-free mechanism can be extended to ghost imaging by comparing the interferometer, which has the detectors on the Fourier transform plane, with ghost imaging, which has the detectors on the imaging plane. On the imaging plane, the path overlap can still be achieved, allowing for measurements insensitive to turbulence. In 2011, Meyers et al. achieved this condition and demonstrated turbulence-free ghost imaging [14]. It should be noted that other types of ghost imaging that have been developed do not have this same property. So far turbulence-free ghost imaging has only been achieved with ghost imaging from intensity fluctuation correlation as a result of two-photon interference. Other types of ghost imaging such as speckle–speckle correlation, computational ghost imaging, and ghost imaging with entangled photons are results of different phenomena, preventing them from being turbulence-free.

4. X-ray ghost imaging

Traditional imaging is dependent on a lens, so will be limited to a certain range of wavelengths. However, we have seen that ghost imaging does not require a lens, so photons with higher energy levels such as X rays can be used. This leads to a substantial increase in image resolution and allows the imaging of more objects due to the higher

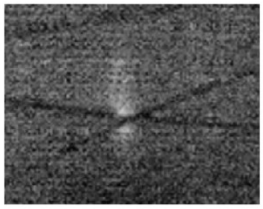

Fig. 3. Preliminary tests used the Advanced Photon Source (APS) at Argonne National Laboratory (ANL) to test spatial resolution capabilities of a LYSO scintillator. Here a traditional image was captured of a 20 micrometer wire. Theoretically, the spatial resolution of a LYSO scintillator may be as low as nanometer or angstrom.

penetrating power of X-rays. Following the Rayleigh criterion [7,13], we find that the minimum spatial separation between resolvable points on the object with ghost imaging is,

$$\Delta x_{GI} \approx \frac{\lambda}{\Delta\theta_s}, \tag{13}$$

where $\Delta\theta_s$ is the angular diameter of the source. As an example of how powerful the use of X rays can be, let us consider hard X rays with a wavelength of 0.05 nm (E ~ 25 keV) and a source with a angular diameter of approximately 0.05 milliradians, which is achievable for many modern X-ray synchrotron sources such as the Advanced Photon Source (APS) at Argonne National Laboratory (ANL). This gives a minimum angular resolution on the order of micrometers, $\Delta x_{GI} \approx 1\times10^{-6}$ m. This is roughly 10,000 times greater image resolution than using visible light (~ 500 nm) with a comparable angular diameter for the source. This improvement can be increased even further with higher energy photons or a larger source, which may be more easily achieved with the implementation of an X-ray tube as a source, but other limitations may arise.

The shift from visible ghost imaging to X-ray ghost imaging may not be trivial. One of the main obstacles is the beam splitter, which is typically trivial for visible light. Currently Bragg or Laue diffraction is used, treating one of the diffracted paths as one path and the transmitted X rays as the other [13]. While functional, this technique is not completely ideal for two reasons: (1) Due to loss of intensity via absorption and other diffraction paths, the efficiency of the imaging process is lowered and (2) the split is often not 50/50 which also reduces the imaging efficiency. Despite these restrictions, diffraction is still the most practical option because of cost and proven functionality. Of interest is the recent development of a kinoform X-ray beam splitter which may prove to be an option for X-ray ghost imaging in the future [15]. Another issue is measuring the intensity fluctuations (via intensity measurements) of the X rays. To accomplish this, it is common to use scintillators to convert the X rays to visible light which can be measured with visible light detectors while certain detector arrays have also been developed with the capability to detect X rays directly. Due to the high resolution of the ghost imaging process, limiting factors for the images will be dependent on the hardware; such as the pixel size for the detector array and potentially the spatial resolution of the scintillator. With recent beam time at the APS we were able to test the spatial resolution of lutetium yttrium oxyorthosilicate (LYSO:Ce) scintillators and can confirm that they are acceptable for ghost imaging at the micrometer level (Fig. 3), and may be able to resolve to the nanometer or angstrom level. LYSO scintillators (as well as many other scintillators) also had decay times shorter than the pulse separation at the APS. This temporal resolution of the scintillator is important to allow for detection of a single pulse, which is preferred for ghost imaging. Further tests are planned which intend to provide understanding of how a scintillator affects the measurement of intensity fluctuations.

In addition to converting X rays to visible photons, scintillators may have a use in permitting magnification in our X-ray ghost imaging setup. Unlike traditional imaging, lensless ghost imaging does not typically result in a magnification factor. To introduce magnification

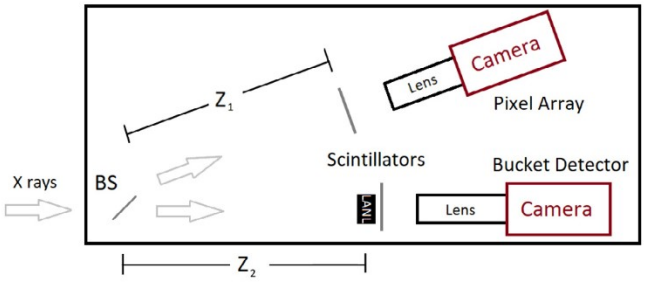

Fig. 4. One setup for X-ray ghost imaging consists of a thermal source of X-ray radiation, a "beam splitter" utilizing Laue diffraction, scintillators, and a pair of cameras. The object, represented here as "LANL", is in the path of the bucket detector and is not seen by the pixel array. The scintillators act as our detection planes and each camera is focused on the corresponding scintillator.

to optical ghost imaging, it is common to use a lens to classically image, and magnify, the ghost image plane [2,14]. This would be useful for X-ray ghost imaging because magnification would allow for higher resolution images to be captured by a single detector array. However, as discussed, the purpose of X-ray ghost imaging was the ability to achieve true point-to-point imaging with X rays, which are unaffected by a lens. To achieve these goals, our plan is to further improve the setup as shown in Fig. 4.

There has been a growing interest in using synchrotrons and other X-ray sources for ghost imaging with results reported by multiple groups [16–22]; however, it appears that these techniques are a result of a classical speckle-to-speckle correlation which does not have the same resolution or turbulence-free capabilities of two-photon interference. Demonstration of true point-to-point imaging from two-photon interference as well as the turbulence-free and other noise immunities of this measurement would be an important step to realize X-ray ghost imaging in a variety of applications.

Acknowledgments

This work is supported by the C2 program, managed by Dr. Dana Dattelbaum at Los Alamos National Laboratory, USA. Z.W. would like to thank Drs. Rich Sheffield and Cris Barnes for interest, support and discussions.

References

[1] T.B. Pittman, Y.H. Shih, D.V. Strekalov, A.V. Sergienko, Optical imaging by means of two-photon quantum entanglement, Phys. Rev. A 52 (1995) R3429.
[2] A. Valencia, G. Scarcelli, M. D'Angelo, Y.H. Shih, Two-photon imaging with thermal light, Phys. Rev. Lett. 94 (2005) 063601.
[3] G. Scarcelli, V. Berardi, Y.H. Shih, Can two-photon correlation of chaotic light be considered as correlation of intensity fluctuations? Phys. Rev. Lett. 96 (2006) 063602.
[4] A. Einstein, Zur elektrodynamik bewegter körper, Ann. Phys. 322 (1905) 891.
[5] R.J. Glauber, Photon correlations, Phys. Rev. Lett. 10 (1963) 84.
[6] R.J. Glauber, The quantum theory of optical coherence, Phys. Rev. 130 (1963) 2529.
[7] Y.H. Shih, An Introduction to Quantum Optics: Photon and Biphoton Physics, first ed., CRC press, Taylor & Francis, London, 2011.
[8] M.O. Scully, M.S. Zubairy, Quantum Optics, Cambridge University Press, Cambridge, England, 1997.
[9] P. Dirac, The Principle of Quantum Mechanics, Oxford University Press, 1930.
[10] R. Hanbury Brown, R.Q. Twiss, Correlation between photons in two coherent beams of light, Nature 177 (1956) 27.
[11] R. Hanbury Brown, R.Q. Twiss, A test of a new type of stellar interferometer on sirius, Nature 178 (1956) 1046.
[12] T.A. Smith, Y.H. Shih, The turbulence-free double-slit interferometer, Phys. Rev. Lett. 120 (2018) 063606.
[13] E. Hecht, Optics, Addison Wesley, Reading, MA, 2002.
[14] R.E. Meyers, K.S. Deacon, Y.H. Shih, Turbulence-free ghost imaging, Appl. Phys. Lett. 98 (2011) 111115.
[15] M. Lebugle, G. Seniutinas, F. Marschall, V.A. Guzenko, D. Grolimund, C. David, Tunable kinoform x-ray beam splitter, Opt. Lett. 42 (2017) 4327.